



Measurement of temperature and pressure distribution during ultrasonic processes by sensor foils from polyvinylidene fluoride

Julia Kosloh¹ · Johannes Sackmann¹ · Sebastian Krabbe¹ · Werner Karl Schomburg¹

Received: 22 February 2018 / Accepted: 5 March 2018 / Published online: 9 March 2018
© Springer-Verlag GmbH Germany, part of Springer Nature 2018

Abstract

Micro and nano structures and systems are generated in polymer surfaces with cycle times of a few seconds by ultrasonic processes such as ultrasonic hot embossing, welding and thermoforming paving the way for a variety of new products. However, measuring temperature and pressure during these processes is very difficult because the polymer is enclosed between an anvil and a sonotrode. Temperature and pressure distribution during ultrasonic processing now have been measured inside of a stack of thermoplastic polymer layers by sensor foils from polyvinylidene fluoride, 55 μm in thickness. The measurements are based on the piezoelectric and pyroelectric effect of polyvinylidene fluoride allowing to achieve resolutions in temperature and pressure of up to ± 1 $^{\circ}\text{C}$ and ± 0.5 kPa, respectively. The achieved resolutions in time and in normal and lateral direction are approximately 1 μs , 60 μm and 1 cm, respectively. The maximum temperature inside a foils stack that could be measured was 73 $^{\circ}\text{C}$ because the sensor foils lost sensitivity when heated up more. Every single oscillation of the polymer was measured as a pressure change. The difference in temperature change and ultrasonic pressure amplitude measured in lateral direction below a sonotrode with outer dimensions of 8×12 cm are approximately 12 $^{\circ}\text{C}$ and 4 kPa, 25 and 60%, respectively, indicating the width required for process windows of ultrasonic processing. Moreover, phase shifts are measurable and thus analysis of oscillation characteristics of sonotrodes were investigated.

1 Introduction

Ultrasonic welding, riveting and punching for decades are well-known industrial processes with widespread applications (Daniels 1965; Shoh 1976; Potente 2004). In recent years, other ultrasonic fabrication processes such as ultrasonic hot embossing and thermoforming have been developed as well enabling the fabrication of micro and nano structures and systems with cycle times of a few seconds (Sackmann et al. 2015; Bae et al. 2017; Liu and Dung 2005; Seo and Park 2012; Tseng and Lin 2012; Šakalys et al. 2016; Lin and Chen 2006; Yu et al. 2009; Qi et al. 2013; Mayer et al. 2012; Mekaru et al. 2007; Khuntontong et al. 2008; Mekaru and Yano 2017; Lee et al. 2010; Altmann et al. 2012; Planellas et al. 2014; Liao et al. 2015).

All these processes are based on friction heat generated by ultrasonic vibrations in thermoplastic polymers.

Obviously, it is of great interest how temperature and pressure evolve during ultrasonic processes and how their distribution is over volume and time inside of a work piece. Investigations have been performed to measure overall and local temperature and pressure during ultrasonic processes (Sun et al. 2011, 2016; Zhang et al. 2010) but it is hard measuring a distribution especially with high time resolution. Sensors need to show small heat capacity and dimensions because they shall not influence the measurement result. This is especially a problem when not only the overall temperature and pressure but the distribution of these parameters shall be determined. In case of ultrasonic welding, optical measurements of previous research showed that polymer welding parts move with the working frequency and its harmonics of ultrasonic welding machines (Habenicht and Ritter 1989). Recently, polyvinylidene fluoride (PVDF) foils have been employed to measure the temperature distribution during ultrasonic hot embossing (Kosloh et al. 2017). In this paper, this method is extended to measure both the temperature and the pressure

✉ Werner Karl Schomburg
Schomburg@KEmikro.rwth-aachen.de

¹ Design and Development of Microsystems (KEmikro),
RWTH Aachen University, Campus-Boulevard 30,
52074 Aachen, Germany

distribution with high time resolution. The method was employed to determine the width of the process window required for ultrasonic processes.

2 Experimental

In this contribution a measurement setup for ultrasonic processes was developed. In the following first ultrasonic processes and its key parameters are described. As shown secondly, a measurement curve recorded with PVDF sensor foils of an ultrasonic process is influenced by both—heat and pressure due to its piezo- and pyroelectric properties. Therefore both effects were calibrated.

2.1 Ultrasonic processing

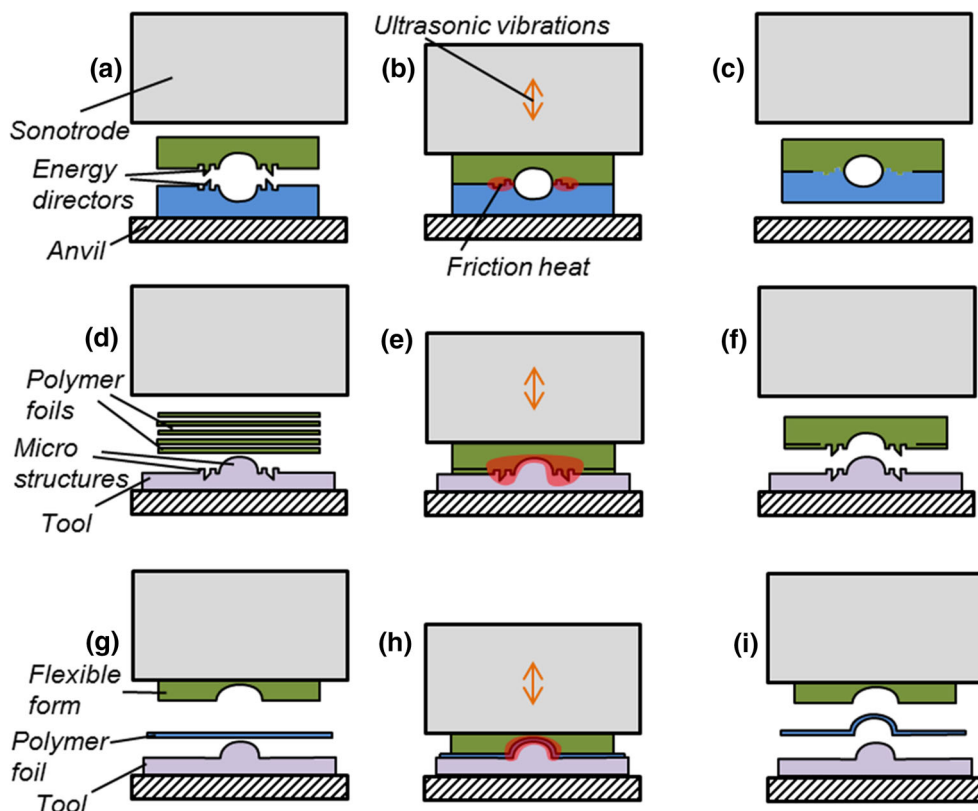
In ultrasonic processing, layers from thermoplastic polymers are placed between the sonotrode of an ultrasonic welding machine and an anvil. For ultrasonic welding (Fig. 1a–c), at least on the surface of one of two polymer parts, there are protruding structures called energy directors facing the other part (Fig. 1a). For ultrasonic hot embossing (Fig. 1d–f), protruding micro structures are on the sonotrode or a tool between anvil and polymer. The thermoplastics to be molded can be applied as foils or as a single plate (Fig. 1d). If a stack of polymer foils is used,

friction heat is generated not only between tool and polymer but also in between the foils (Sackmann et al. 2015). For ultrasonic thermoforming (Fig. 1g–i), on the side of the polymer opposite to the tool, there is fixed some flexible material possibly also with a micro structure inverse to the one on the tool in order to pattern the single polymer foil (Fig. 1g). Instead of such a flexible material, it is possible to apply a stack of polymer foils from a polymer which cannot be welded together with the foil to be thermoformed (Sackmann et al. 2015).

The sonotrode is pressed down onto the polymer and ultrasonic vibrations are transmitted by it into the polymer. Friction heat generated by the vibrations melts the polymer which is adapting to the surrounding geometry (Fig. 1b, e, h). After switching off the ultrasound, the polymer is solidifying again and the product of the process is taken out of the equipment (Fig. 1c, f, i). The common advantage of all these processes is that only a small amount of polymer is molten, and therefore, the cycle time is in the order of seconds (Sackmann et al. 2015). In Fig. 2 an ultrasonically structured PC-foil (a) and an ultrasonically hot embossed PEEK-microchannel are shown.

Since the vibration amplitude of the sonotrode is not homogeneous over its surface, the process window of the ultrasonic processes needs to be large enough to work everywhere on a larger work piece. Otherwise, a part of the polymer may be not yet molten while at another position it

Fig. 1 Schematic drawing of ultrasonic processes: **a–c** welding, **d–f** hot embossing, and **g–i** thermoforming



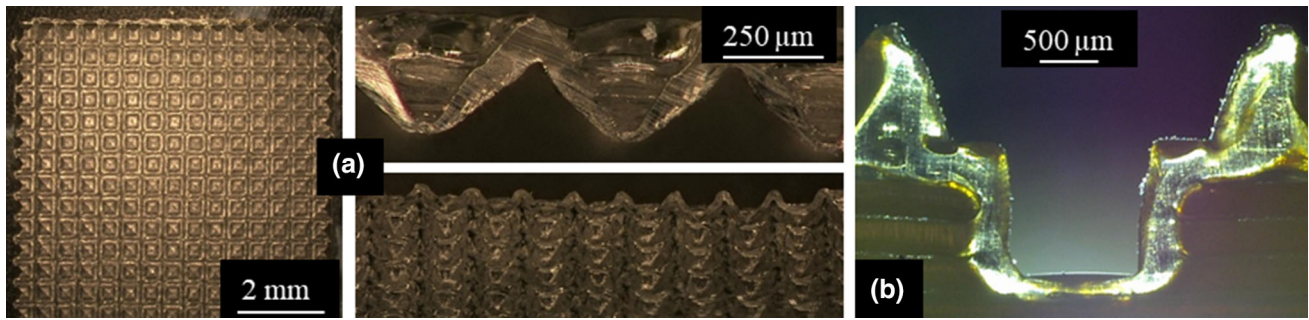


Fig. 2 **a** Ultrasonically thermoformed 125 μm thick PC-foil (structured at both sides with micro pyramids), **b** a thin (less than 500 μm) cut through an ultrasonically hot embossed microchannel from semi

crystalline PEEK (transparent areas became amorphous due to the ultrasonic treatment)

is already decomposed due to overheating or the molten polymer has already flown to a position where it is not desired. That is why temperature and pressure distribution are interesting to be known.

Parameters of ultrasonic processes of the following experiments are shown in Table 1 below.

2.2 Measurement setup and calibration

The polymer polyvinylidene fluoride (PVDF) can be made piezoelectric during fabrication. Besides other shapes, it is commercially available as thin foils covered with electrodes on both sides. If a PVDF foil is compressed by a force, electrical charges are generated on the electrodes and a voltage proportional to the applied force can be measured (Shirinov and Schomburg 2008; Schomburg 2015). This is the so-called piezoelectric d_{33} -effect. Thus, PVDF foils can be employed as force or pressure sensors. If a PVDF foil is stretched in longitudinal direction, there is also a piezoelectric effect, the so-called d_{31} -effect (Schomburg 2015), but the sign of the measured voltage is opposite to the d_{33} -effect. Whether the measured voltage is positive or negative is also a function of the polarization of the foil and the

electronics employed for measurement. Important for the following is only that the sign of the measured voltage is opposite for d_{31} - and d_{33} -effect. Besides the piezoelectric effect, PVDF is also pyroelectric (Shirinov and Schomburg 2008; Schomburg 2015). That means that a temperature change also results in charges generated on the electrodes. A rising temperature results in a voltage with a sign opposite to the one generated by compressing the foil perpendicular to its surface.

For the measurements, a buffer amplifier circuit was used (Shirinov and Schomburg 2008), see Fig. 3. For the output signal recording, three DAQ-boxes (type: NI Elvis II +) from National Instruments were used. For a high sampling rate and in order to reduce ghosting, each box was connected to a single PVDF-sensor. Thus, measurements with three sensors could be done simultaneously. The starting time of the measurements with all three boxes was synchronously. This was achieved by a common clock signal for all boxes, the same trigger signal, and the maximum sample rate of 1 MS/s (10^6 samples/s) was set for each box. Thus, it was possible to even calculate phase shifts from the measured data. In this publication, the measured data were processed and evaluated (e.g. filter

Table 1 Parameters and machine settings of ultrasonic fabrication processes

Process number	1	2	3	4
Ultrasonic welding machine ^a	1	3	3	2
Working frequency (kHz)	35	20	20	35
Sonotrode dimensions (mm ²)	40 × 60	80 × 120	80 × 120	40 × 60
Trigger force (factor × F _w)	~ 1	~ 0.9	~ 0.9	~ 0.8
Force during vibrations, F _w (N)	100	Varied	800	Varied
Amplitude of vibration (μm)	7.7	30.6	30.6	16.3
Duration of vibrations (s)	50	Varied	200	1000
Cooling time (s)	1500	Varied	4000	1000
Capacity C ₀ (nC)	47	47	47	–
Voltage divider: yes/no	No	Yes	Yes	–

^aWelding machines: (1) Dynamic 745 from Rinco Ultrasonics, Switzerland, (2) HiQ DIALOG 1200 from Herrmann Ultrasonics, Germany, (3) HiQ DIALOG 6200 from Herrmann Ultrasonics, Germany

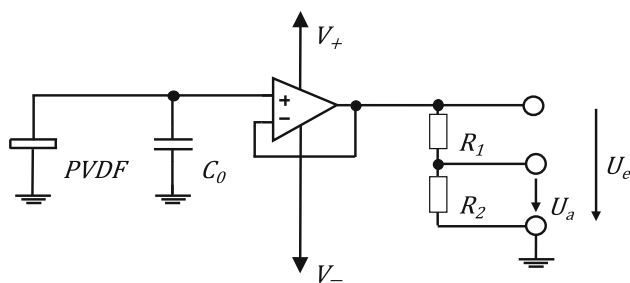


Fig. 3 Schematic drawing of applied circuit

design, peak detection, Fourier analysis) with the program Matlab from the MathWorks Inc.

In Fig. 4, a foils stack with an integrated PVDF sensor foil is shown. Such an arrangement of foils is conceivable for different ultrasonic processes.

In Fig. 5 there is shown the voltage signal recorded during ultrasonic processing of a stack with a PC foil and a plate as shown in Fig. 4 with the parameters shown in Table 1 as process 1. When the sonotrode touches the polymer stack (decreasing voltage in Fig. 5), on the one hand pressure is built up, and on the other hand the temperature may change (increasing voltage in Fig. 5) because the sonotrode may be at a higher temperature than the polymer layers. After, the sonotrode touches down and a force is build up, the ultrasound starts and due to the generated heat a positive voltage shift is detectable (also called pyroelectric shift). After the ultrasound is switched off, the foils stack cools down and the process ends with the lift off of the sonotrode which is clearly detectable due to the piezoelectric effect. After the ultrasonic vibrations are switched off, the temperature is decreasing due to dissipation of the heat into anvil and sonotrode. When the sonotrode is moved up again, the release of the load is seen in the data and the temperature decrease is slowed down because heat dissipation can no longer go into the sonotrode.

Since high output voltages can occur with such sensor foils, it is necessary to apply large capacities C_0 (see Fig. 3) which are connected in parallel to the one of the PVDF-Sensor foil (type: FDT1-028K). Important for the

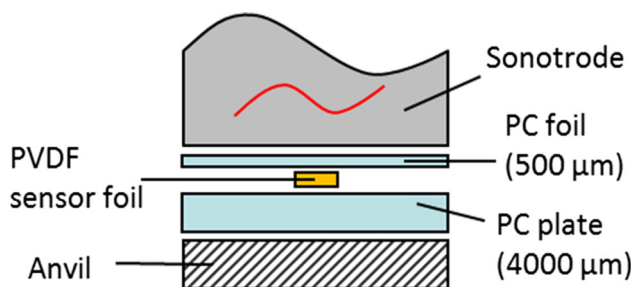


Fig. 4 Foils stack with PVDF sensor foil for process 1

following validation is that the capacity C_0 was never less than 47 nF and thus it was much larger than the capacity of the PVDF-sensor which is 1.37 nF according to the manufacturer Measurement Specialities. But sometimes it was necessary to connect higher capacities such as 100 nF in parallel because the charges were so high that the voltage was exceeding the possible input range of the operational amplifiers which was set to + 25 V and to - 10 V. As operational amplifiers, amplifiers with a gain factor of 1 (type: CA3140), were used to provide a high input impedance and a low input current. Moreover, a voltage divider ($R_1 = 1 \text{ M}\Omega$ and $R_2 = 660 \text{ k}\Omega$) was used optionally if the resulting output voltage was higher than the admitted maximal input voltage of the DAQ-boxes which is $\pm 10 \text{ V}$ according to the manufacturer National Instruments. The maximal output voltage of the operational amplifiers is $\sim 3 \text{ V}$ below its supply voltage which was set to + 25 V in the presented experiments. Thus, the maximal resulting 22 V was multiplied with the factor 0.4 by the voltage divider to gain 8.8 V ($22 \text{ V} \times 0.4 = 8.8 \text{ V}$) which is with an adequate buffer small enough as input voltage for the DAQ-Boxes.

All in all, it is preferable in some cases to calculate the charge change q instead of the output voltage U_a . Voltage changes were measured and converted into charge changes (assuming $C_{\text{PVDF}} = \text{const} = 1.37 \text{ nF}$) by the following equation (Shirinov and Schomburg 2008):

$$q = (C_0 + C_{\text{PVDF}}) U_e = (C_0 + C_{\text{PVDF}}) \frac{R_2 + R_1}{R_2} U_a \quad (1)$$

For an ultrasonic hot embossing process, both the temperature change and the pressure change affect the output voltage and thus the charge change (Kosloh et al. 2017). Therefore, both effects have to be calibrated and that was done as follows.

The pressure change and thus the voltage change due to the piezoelectric effect was calibrated by applying different pressures to one sensor. The sensor was placed between two plates from thermoplastic polyurethane (TPU) and different forces were applied by an ultrasonic welding machine without ultrasonic vibrations. Elastic 2 mm-thick TPU (Desmopan 192 from the Covestro AG) was used, because this leads to a homogenous (as good as possible) pressure distribution under the sonotrode. The pressure was calculated by dividing the applied force by the area of the sonotrode which was $4 \times 6 \text{ cm}^2$. Figure 6 shows the charge generated by a pressure increase due to applied forces by the ultrasonic welding machine. C_0 was 47 nF.

A fit to the data yields the pressure change Δp as a function of the measured charge q_p and the charge generated by a pressure change:

Fig. 5 Example for typical measurement curves

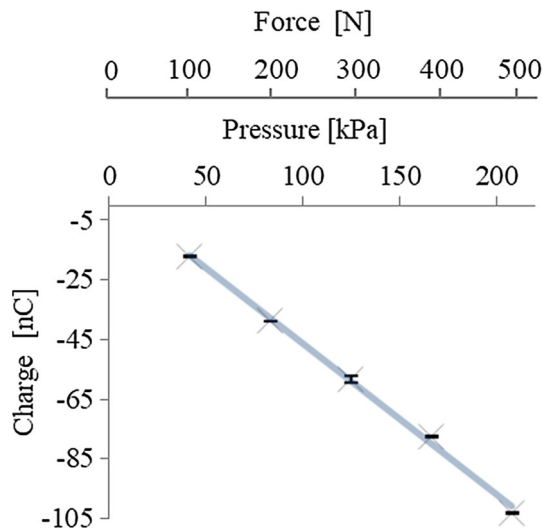
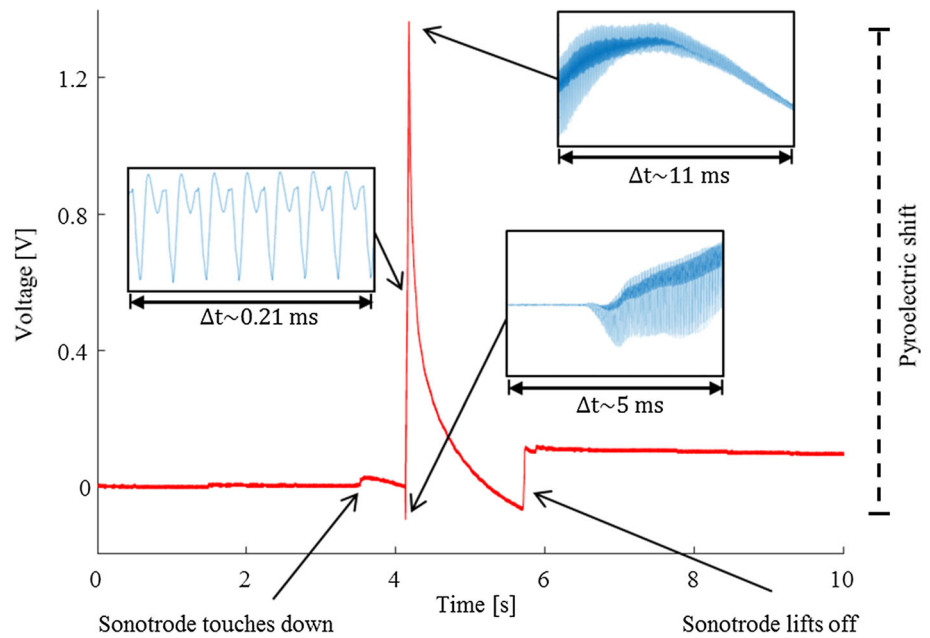


Fig. 6 Charge generated by the piezoelectric effect of PVDF foils as a function of pressure load according to a set force at the ultrasonic welding machine, respectively. Shown are mean values and standard deviations of two measurements in each case

$$\Delta p = -1.98 \times 10^3 q_p \frac{Pa}{nC} \tag{2}$$

$$q_p = -0.51 \times 10^{-3} \Delta p \frac{nC}{Pa} \tag{3}$$

The temperature change was calibrated by immersing the PVDF sensor foils into a bath of oil and measuring the charge change q_T as a function of the difference of oil and ambient temperature ΔT . The measured charges 5 s after immersing into the oil bath are shown in Fig. 7 as a function of the bath temperature. The room temperature was 23.8 °C. C_0 was 100 nF.

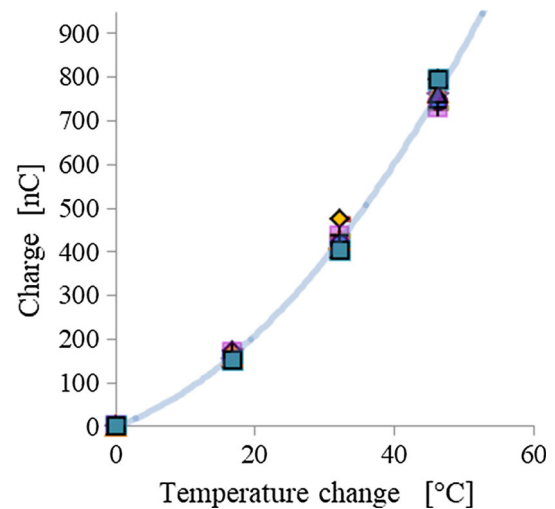


Fig. 7 Charge generated by the pyroelectric effect of five PVDF foils as a function of temperature change. Shown are measured values of five sensors in each case

The following calibration curve and its nonlinear approximation result:

$$\Delta T = -12.4 \text{ } ^\circ\text{C} + \sqrt{154 \text{ } ^\circ\text{C}^2 + 4.29 q_T \frac{^\circ\text{C}^2}{nC}} \tag{4}$$

$$q_T = 5.8 \times \Delta T \frac{nC}{^\circ\text{C}} + 0.23 \times \Delta T^2 \frac{nC}{^\circ\text{C}^2} \tag{5}$$

Obviously, an ultrasonic process implies on the one hand pressure changes due to a welding or an embossing force and moreover due to the ultrasonic vibrations, and on the other hand temperature changes to melt the polymer.

All in all, charge changes q_i are summarized by the following equation:

$$q_T + q_p = 5.8 \times \Delta T \frac{nC}{^\circ C} + 0.23 \times \Delta T^2 \frac{nC}{^\circ C^2} - 0.51 \times 10^{-3} \Delta p \frac{nC}{Pa} \quad (6)$$

The measurement range is limited by the Curie temperature of the PVDF. Therefore, the ultrasonic power needed to be limited such that not more than approximately 80 °C were reached at the sensor foils, which is recommended by the manufacturer of the sensors. Thus for most polymers, it is not possible to measure at their softening temperature where ultrasonic hot embossing and welding are usually performed. On the other hand, measurements can reveal the relative distribution of heat generation and ultrasonic amplitude at lower power which is expected to be similar as at higher power.

3 Results and discussion

The results presented here show how ultrasonic processes can be analyzed, e.g. oscillation spectra of ultrasonic vibrations in foils stacks and ways to determine heat and pressure distribution in ultrasonic processes. Finally these distributions were measured in lateral direction and reproducibility studies were performed.

3.1 Signal analysis of ultrasonic processes

Figure 8 shows frequency spectra of signals measured during ultrasonic processing. The signals were obtained from the ultrasonic welding machines 1 and 3, see Table 1, working at 35 and 20 kHz, respectively:

These spectra show the ultrasonic welding frequencies 20 and 35 kHz and their harmonics 40, 60 kHz, etc. and 70, 105 kHz, etc., respectively. The frequency peaks shown in Fig. 8 are all due to the mechanical vibrations and the piezoelectric effect because the temperature rise generated by friction heat is much slower and would correspond to a frequency of approximately 10 Hz (see below).

Thus, pyroelectric and piezoelectric effect can be distinguished in this application by their frequencies. In Fig. 9, it is shown that the original signal can be separated into the pyroelectric shift with a low pass filter and the piezoelectric ultrasonic oscillation with a high pass filter.

When ultrasonic vibrations are starting, both the pressure changes are recognized in the signal and there is seen a general increase of the voltage due to the rising temperature generated by friction heat, see Fig. 9a. The part of the signal recorded during ultrasonic vibrations was applied to

a low pass filter with stop band and pass band of 9 and 1 kHz, respectively. Assuming ideal filter characteristics, this means that frequencies below a cutoff frequency between 1 and 9 kHz can perfectly pass while frequencies above this cutoff frequency are perfectly suppressed (Antoniou 2009). The result of this calculation is shown in Fig. 9b. The high frequency vibrations were removed from the signal and only the signal change due to the temperature change is seen. From this signal the temperature change can be calculated by Eqs. (1) and (4).

The part of the signal recorded during ultrasonic vibrations was also applied to a high pass filter with stop band and pass band of 9 and 14 kHz, respectively. As a consequence, all frequencies below 9 kHz were suppressed and frequencies above 14 kHz were not altered, again assuming ideal filter characteristics (Antoniou 2009). The result of this calculation is shown in Fig. 9c and contains only the mechanical vibrations. It is seen that there was not a pure sine wave at 35 kHz but that it was superimposed by a vibration at 70 kHz. This signal can be employed to calculate the amplitude of the pressure change generated in the polymer stack by Eqs. (1) and (2).

It was observed that the result of the temperature change and vibration amplitude obtained as described above is a function of stop band and pass band parameters, since the transfer function of practical filters differs from ideal filters and may lead to amplitude distortion (Antoniou 2009). To avoid this ambiguity in the following experiments, the vibration amplitudes were taken directly from the signal shown in Fig. 9a. The vibration amplitude was calculated by averaging all peak-to-peak-amplitudes of the ultrasonic oscillation of a pyroelectric shift and applying Eqs. (1) and (2). The temperature change was determined from the change of the mean value between maxima and minima of the vibrations observed in Fig. 9a. Therefore, the vibration oscillations were removed from the pyroelectric shift: The mean value between the peak-to-peak values was determined for each oscillation of this signal part (cf. Fig. 10) and the temperature change was determined from the resulting smoothed signal part (cf. Fig. 10, black graph) and applying Eqs. (1) and (4).

3.2 Heat and pressure distribution in lateral direction

The measurement approach described above was employed to determine the distribution of temperature and pressure amplitude during ultrasonic processing. Three PVDF sensor foils were placed in the center and 12.5 mm from the rim of a sonotrode with $8 \times 12 \text{ cm}^2$ contact area into a stack of three not piezoelectric PVDF foils, each 250 μm in thickness (cf. Fig. 11). The sensor foils had a sensitive area of $12 \times 30 \text{ mm}^2$ and were placed below the not

Fig. 8 Frequency spectrum of PVDF sensors in a foils stack while applying ultrasonic vibrations at 35 kHz (a) and 20 kHz (b), respectively. Spectra were calculated from 15 ms of the signal obtained during the vibrations of processes 1 and 2 in Table 1

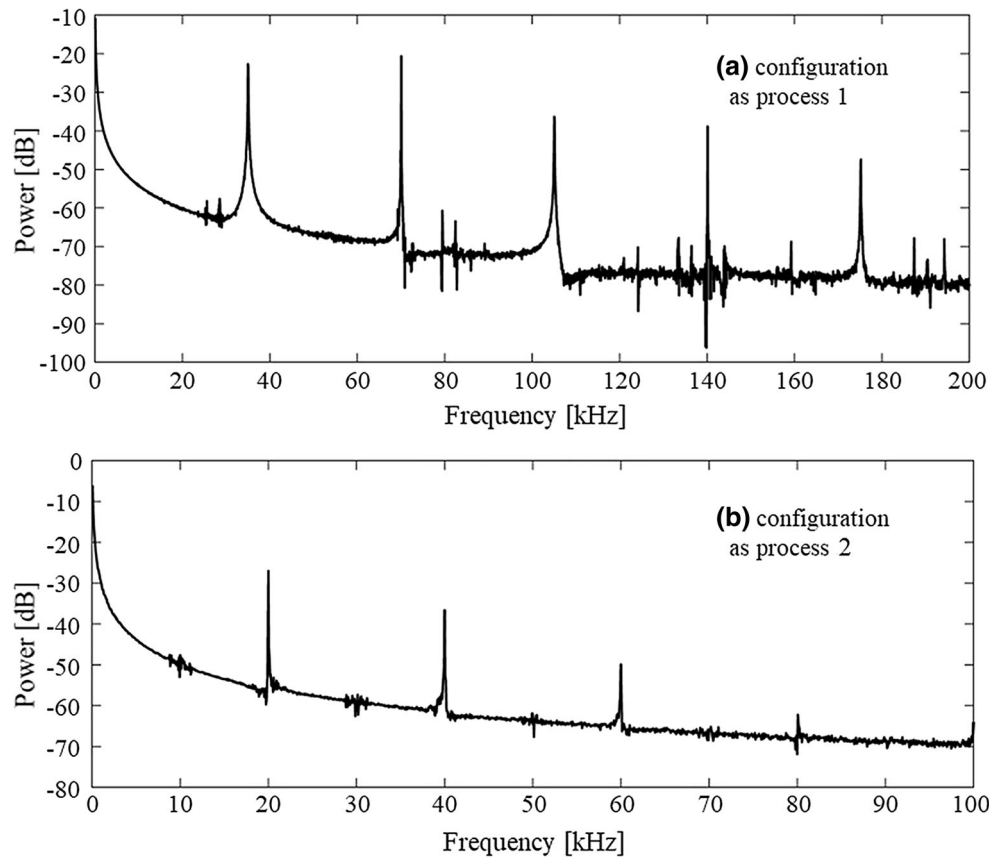
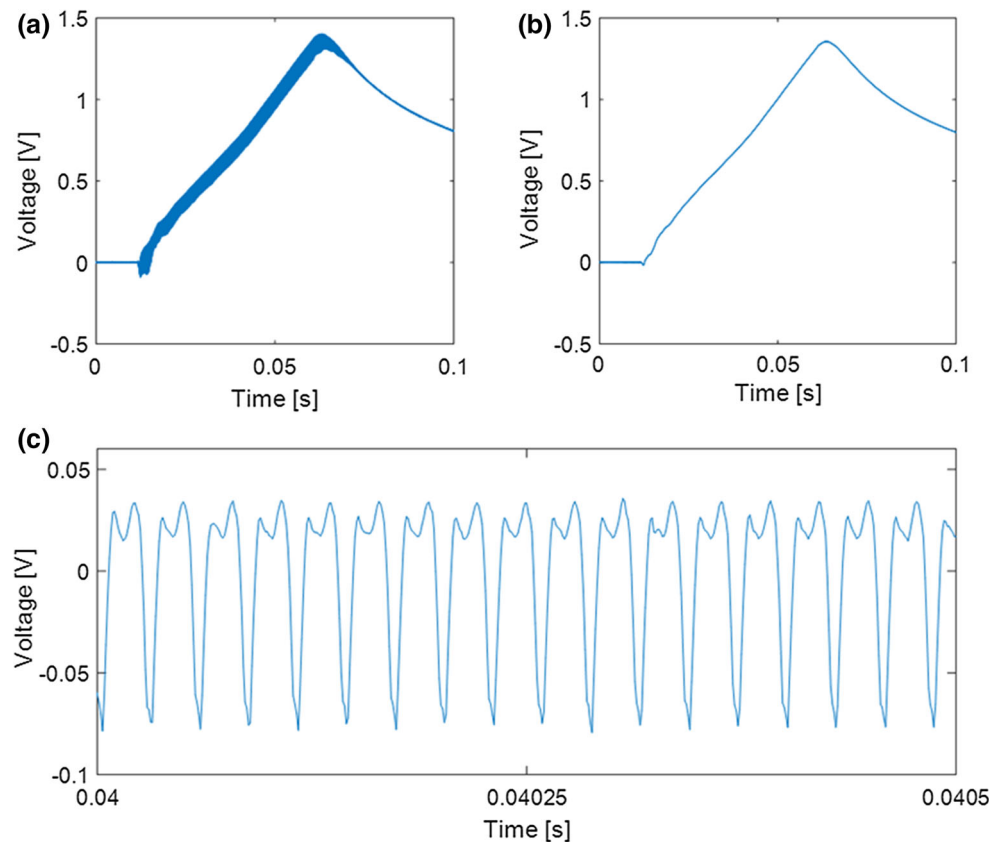


Fig. 9 Original signal (process 1 in Table 1) of a pyroelectric shift (a), filtered with a low pass filter (b), and filtered with a high pass (c)



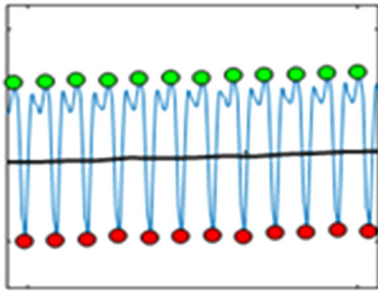
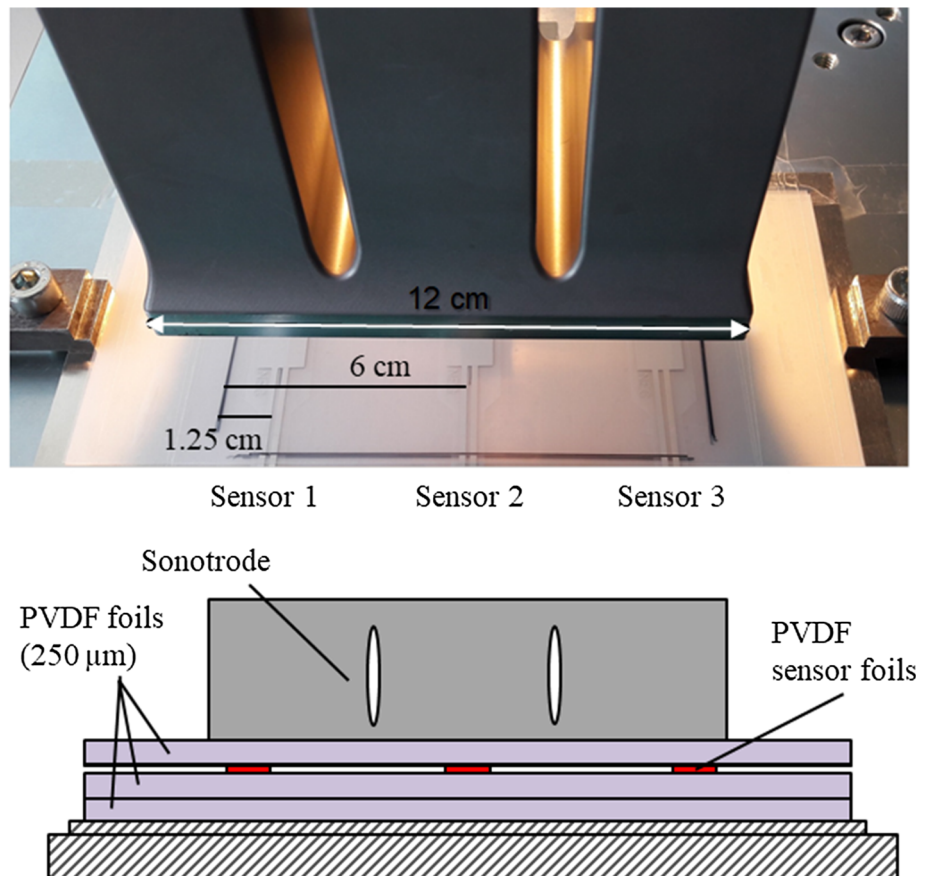


Fig. 10 Adjusted signal

piezoelectric foil in contact with the sonotrode. All experiments were performed with the ultrasonic welding machine 3 tuned to $30.6\ \mu\text{m}$ vibration amplitude of the sonotrode. The electronics of the machine tries to retain this amplitude when the sonotrode is pressed onto the polymer stack. For the following experiments the foils stack including the PVDF sensor was never removed or disassembled so that always the same foils and the same sensor were used for each measurement.

The temperature measured in the stack is shown in Fig. 12 for pressing forces between 150 and 800 N and after different times of ultrasonic vibrations (process 2 in Table 1 with the machine settings: 50, 100 and 200 ms

Fig. 11 Photo and schematic drawing of the setup for process 2 and 3 in Table 1 employed for the measurement of temperature and pressure distribution



durations of vibrations). At 150 N and 100 ms time of ultrasonic vibrations, within the error bars the temperature is the same at all measurement positions. At 800 N and 50 ms the temperature change is approximately 25% larger in the center of the sonotrode than at the rim. With a time of 50 ms of ultrasonic vibration, the temperature is raised by approximately $5\ ^\circ\text{C}$ but in an ultrasonic process with a longer time of 200 ms of ultrasonic vibrations in the center of the sonotrode the sensor foil already arrives at $73\ ^\circ\text{C}$.

The pressure amplitudes corresponding to the temperature measurements shown in Fig. 12 are displayed in Fig. 13. The amplitude of the pressure vibrations below the center of the sonotrode is approximately 60% larger than at the rim for a pressing force of 800 N. This explains why the generated friction heat as shown in Fig. 12 is larger below the center of the sonotrode than below its rim. When the pressing force is only 150 N, the vibrations generate less friction heat than at 800 N. Amplitudes of the pressure vibrations were also calculated after filtering the signal with a bandpass filter. The bandpass filter was designed with a middle frequency of 20 kHz which was the working frequency of the ultrasonic welding machine in this process. The pass bands were 15 and 25 kHz and the stop bands were 10 and 30 kHz, respectively. Peak-to-peak-amplitudes of pressure vibrations with the machine

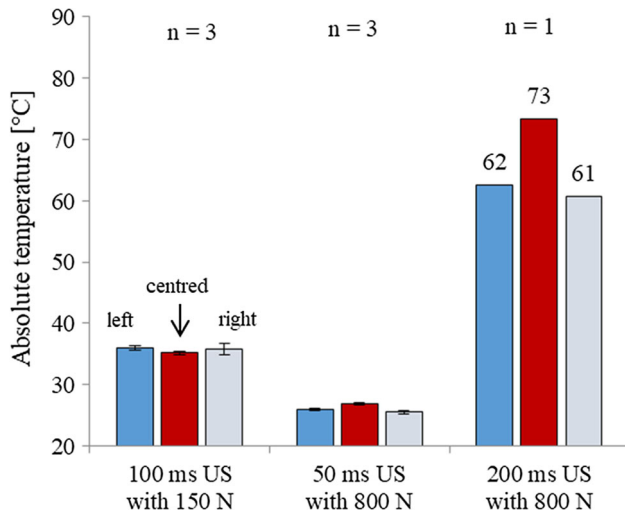


Fig. 12 Absolute temperatures, calculated from measured and evaluated temperature shifts ΔT plus the ambient temperature (21.4 °C) below the center and the sides of the sonotrode at different pressing forces and times of ultrasonic vibrations. Shown are mean values and standard deviations of three pyroelectric measurements in each case with the exception of the last three bars because the temperatures reached nearly the maximum operating temperature of the sensors and therefore equal conditions were no longer ensured

working frequency are smaller, but show the same characteristics.

Vibration amplitudes were also measured with a microscope at the side of a sonotrode (Fig. 14a), see process 4 in Table 1. Pictures were taken near the lower edge (less than 2 mm) of the sonotrode. In the pictures recorded with the microscope structures on the surface of the

sonotrode near to the foils stack were present. The foils stack was built from five PP-foils, each foil was 200 μm thick. When the sonotrode is vibrating, the structures are visible as strait lines and the length of these lines is the amplitude of the vibrations (Fig. 14b).

The mean values of the measured amplitudes and their standard deviations are shown in Fig. 15. There were always made several photos with the microscope and approximately four measurements were taken from each photo.

At the rim of the sonotrode, all measured amplitudes were more than 18% smaller than the ultrasonic welding machine was tuned to. It may be that in the center of the sonotrode the real amplitude was the same as adjusted at the machine.

The amplitude at the corner of the sonotrode turned out to be approximately 7–9% larger than in the middle of the longer edge. Besides this, it is seen that the amplitude is not much influenced by the force with which the sonotrode is pressed onto the polymer stack. This is caused by the control system of the machine keeping the amplitude constant.

With the PVDF foils, it is also possible to measure the phase difference of the vibrations at the center and the rim of sonotrodes. In Fig. 16, there are shown the output voltages of the three PVDF foils filtered with a bandpass filter as a function of time. The bandpass filter was designed with a middle frequency of 20 kHz which was the working frequency of the ultrasonic welding machine in this process, the pass bands were 15 and 25 kHz and the

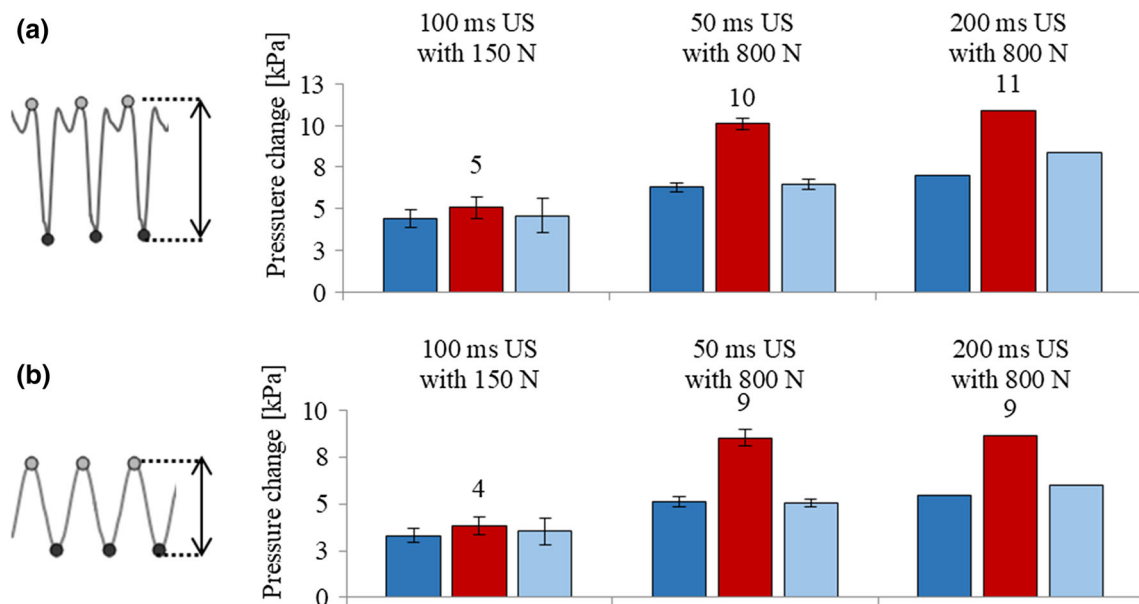


Fig. 13 Averaged peak-to-peak-amplitudes of pressure vibrations during pyroelectric shift measured below the center and the sides of the sonotrode for processes with different pressing forces and times of

ultrasonic vibrations: **a** original signal, **b** bandpass filtered signal. Shown are mean values and standard deviations of three ultrasonic experiments in each case with the exception of the last three bars

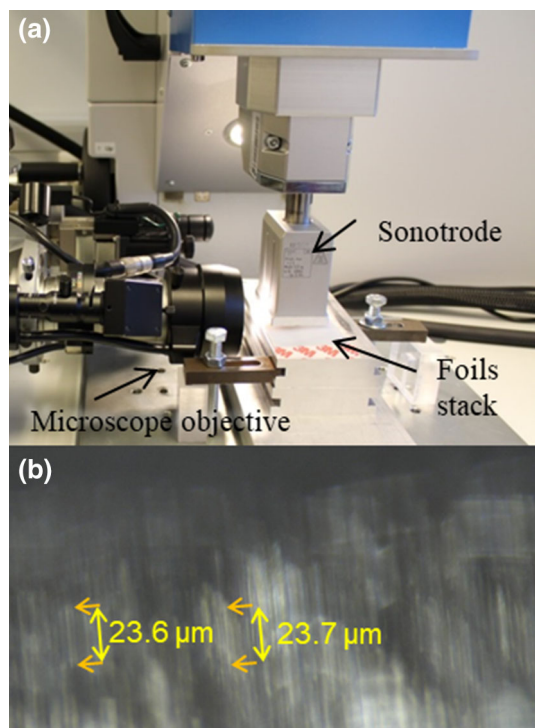


Fig. 14 Measurement of vibration amplitude with a microscope at the edge of the sonotrode

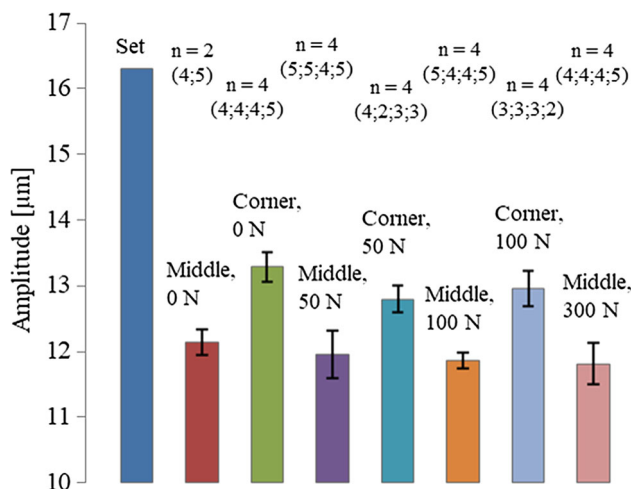


Fig. 15 Vibration peak amplitudes measured at different positions at the edge of a sonotrode. *n* is the number of photos which were taken in different processes. *n* = 3 (1, 2, 4) means three photos were taken and 1, 2 and 4 measurements of vibration amplitudes were done in the first, second and third photo, respectively

stop bands were 10 and 30 kHz, respectively. It is clearly seen that there is a phase difference of approximately $2 \mu\text{s}$ between the vibration at the center of the sonotrode and at the rim at this moment. The foils stack was shown in Fig. 11 and the set parameters can be seen in Table 1, process 3.

3.3 Reproducibility of ultrasonic processes

It had been observed that suitable parameters for ultrasonic hot embossing were changing as a function of time. Therefore, the temperature change ΔT inside of the polymer foils stack from PC shown in Fig. 4 was measured by the pyroelectric effect of a PVDF foil after 50 ms of ultrasonic vibrations with $7.7 \mu\text{m}$ amplitude and a force of 100 N (process 1 in Table 1) on 11 different days of the year and ambient temperature and relative humidity were recorded. Always the same foils stack including the PVDF sensor was used and never removed or disassembled in order to keep equal conditions for each experiment. Absolute temperature can be calculated by adding the ambient temperature to the temperature change ΔT . Figure 17 shows the measurement results obtained on 20 series of tests in the 11 days. ΔT and ambient temperature are shown on the left. The measured pyroelectric shifts as a function of room temperature is shown in Fig. 17 on the right. It is clearly seen that there is a correlation between ambient temperature and the pyroelectric shift and thus between the room temperature and the temperature change ΔT inside of the polymer stack, respectively.

Therefore, it is obvious that room temperature affects the result of ultrasonic processes such as ultrasonic hot embossing and welding. As a consequence, it is suggested that the polymer temperature should be controlled for such processes, for instance by preheating the polymer to a well-defined temperature.

No clear correlation was found between the temperature inside of the polymer stack and relative humidity, see Table 2. But a clear correlation was found between the measured pyroelectric shift and the ambient temperature, see Table 2.

4 Conclusions

Ultrasonic processes like thermoforming, hot embossing and welding have already widespread applications and it is of great interest how temperature and pressure amplitude evolve during ultrasonic treatments. PVDF sensor foils have been employed to measure both pressure and temperature distribution during ultrasonic processing. Because the sensors can be placed anywhere in the foils stack, the heat and pressure distribution can be measured in lateral and normal direction during ultrasonic treatments. Even the ultrasonic pressure amplitude in the polymer foils stack was calculated and the phase shift of vibrations both as a function of position below a sonotrode and as a function of time was observed. This may be helpful for the

Fig. 16 Bandpass filtered output voltages of three PVDF foils during process 3 in Table 1

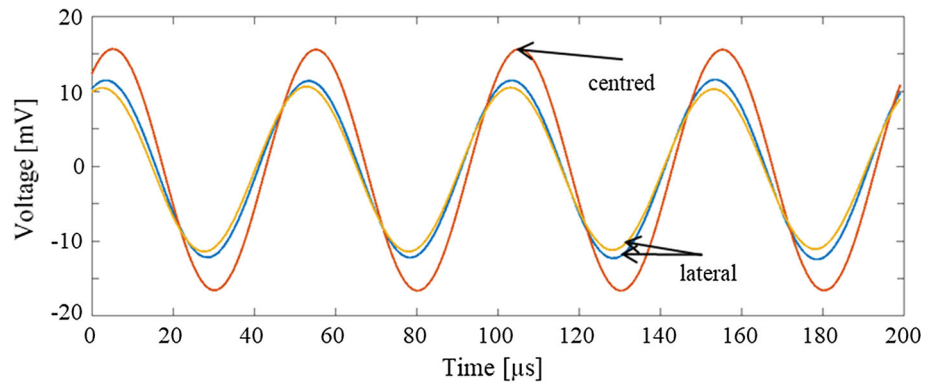


Fig. 17 Temperature changes measured by PVDF foils inside of the polymer stack after 50 ms of ultrasonic vibrations on different days and at different room temperatures (left) and correlation between pyroelectric shift and ambient temperature (right). Shown are mean values and standard deviations of three evaluated pyroelectric measurements in each case

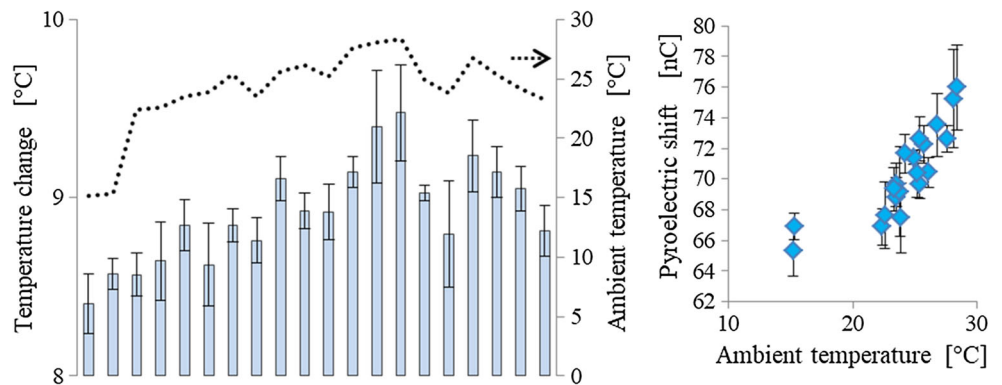


Table 2 Correlation coefficients

	Humidity (%)	Ambient temperature (°C)
Pyroelectric shift (V)/(nC)	- 0.33	0.83

development of both ultrasonic welding machines and ultrasonic processes.

The measurement with PVDF foils is limited by the Curie temperature of the material. As a consequence, reliable measurements can be performed only up to approximately 80 °C. Since melting of thermoplastic polymers occurs typically at higher temperatures, the PVDF foil may be placed a bit farther from the position where the melting takes place or a measurement is performed at less pressing force of a lower ultrasonic amplitude to determine temperature and pressure distribution at lower temperatures.

Acknowledgements The results presented here were partly achieved with the support of Deutsche Forschungsgemeinschaft (DFG) with the support codes SCHO 850/14-1 and SCHO 850/4. Many thanks for supporting the optical measurements of sonotrode amplitudes to Mr. Janhsens.

References

Altmann B, Ahrens R, Welle A, Dinglreiter H, Schneider M, Schober A (2012) Microstructuring of multiwell plates for three-

dimensional cell culture applications by ultrasonic embossing. *Biomed Microdevices* 14:291–301

Antoniou A (2009) Section I passive filters general characteristics of filters. In: Chen W-K (ed) *Passive, active, and digital filters—the circuits and filters handbook*, 3rd edn. CRC Press, Boca Raton

Bae H-J, Lee H-J, Park K (2017) Ultrasonic assisted thermoforming for rapid fabrication of a microspeaker diaphragm. *Microsyst Technol* 23:1677–1686

Daniels HPC (1965) Ultrasonic welding. *Ultrasonics* 3:190–196

Habenicht G, Ritter J (1989) Ultraschallschweißen von thermoplasten. *Kunststoffe* 79:857–860

Khuntontong P, Blaser T, Schomburg WK (2008) Ultrasonic micro hot embossing of thermoplastic polymers. In: *Proceedings of the 24th annual meeting of the Polymer Processing Society, PPS24, Salerno, 15–19 June 2008*, p II.364

Kosloh J, Sackmann J, Šakalys R, Liao S, Gerhardy C, Schomburg WK (2017) Heat generation and distribution in the ultrasonic hot embossing process. *Microsyst Technol* 23:1411–1421

Lee CH, Jung PG, Lee SM, Park SH, Shin BS, Kim J-H, Hwang K-Y, Kim KM, Ko JS (2010) Replication of polyethylene nano-micro hierarchical structures using ultrasonic forming. *J Micromech Microeng* 20(3):035018

Liao S, Gerhardy C, Sackmann J, Schomburg WK (2015) Tools for ultrasonic hot embossing. *Microsyst Technol* 21:1533–1541

Lin C-H, Chen R (2006) Ultrasonic nanoimprint lithography: a new approach to nanopatterning. *J Micro/Nanolithogr MEMS MOEMS* 5(1):011003

- Liu S-J, Dung Y-T (2005) Hot embossing precise structure onto plastic plates by ultrasonic vibration. *Polym Eng Sci* 45:915–925
- Mayer A, Dhima K, Möllenbeck S, Wang S, Scheer H-C (2012) A novel tool for frequency assisted thermal nanoimprint (T-NIL). *Proc. SPIE* 8352, 28th European Mask and Lithography Conference, 83520N (17 April 2012). <https://doi.org/10.1117/12.918037>
- Mekaru H, Yano T (2017) Comparative evaluation of detachable mold fixing methods aimed at low energy loss for ultrasonic nanoimprint lithography. *Microsyst Technol* 23:2707–2717
- Mekaru H, Goto H, Takahashi M (2007) Development of ultrasonic micro hot embossing technology. *Microelectron Eng* 84:1282–1287
- Planellas M, Sacristán M, Rey L, Olmo C, Aymamí J, Casas MT, del Valle LJ, Franco L, Puiggalí J (2014) Micro-molding with ultrasonic vibration energy: new method to disperse nanoclays in polymer matrices. *Ultrason Sonochem* 21(4):1557–1569
- Potente H (2004) *Fügen von Kunststoffen—Grundlagen, Verfahren, Anwendung*. Carl Hanser, München
- Qi N, Luo Y, Yan X, Wang X, Wang L (2013) Using silicon molds for ultrasonic embossing on polymethyl methacrylate (PMMA) substrates. *Microsyst Technol* 19:609–616
- Sackmann J, Burlage K, Gerhardy C, Memering B, Liao S, Schomburg WK (2015) Review on ultrasonic fabrication of polymer micro devices. *Ultrasonics* 56:189–200
- Šakalys R, Janušas G, Palevičius A, Čekas E, Jūrėnas V, Sodah A (2016) Microstructures replication using high frequency excitation. *Microsyst Technol* 22:1831–1843
- Schomburg WK (2015) *Introduction to microsystem design*, 2nd edn. Springer, Heidelberg
- Seo Y, Park K (2012) Direct patterning of micro-features on a polymer substrate using ultrasonic vibration. *Microsyst Technol* 18:2053–2061
- Shirinov AV, Schomburg WK (2008) Pressure sensor from a PVDF film. *Sens Actuators A* 142:48–55
- Shoh A (1976) Welding of thermoplastics by ultrasound. *Ultrasonics* 14:209–217
- Sun Y, Luo Y, Wang X, Zhang M, Feng Y (2011) A new ultrasonic precise bonding method with ultrasound propagation feedback for polymer MEMS. *Microelectron Eng* 88:3049–3053
- Sun Y, Wang F, Li F, Yang X (2016) Study on vibration transmission and interfacial fusion in ultrasonic bonding process for thermoplastic micro joint. *Adv Polym Technol*. <https://doi.org/10.1002/adv.21780>
- Tseng P, Lin C (2012) Impacts of mold material and pattern size for ultrasonic nanoimprint lithography. *Microelectron Eng* 98:112–116
- Yu HW, Lee CH, Jung PG, Shin BS, Kim J-H, Hwang K-Y, Ko JS (2009) Polymer microreplication using ultrasonic vibration energy. *J Micro/Nanolithogr MEMS MOEMS* 8(2):021113
- Zhang Z, Wang X, Luo Y, Zhang Z, Wang L (2010) Study on heating process of ultrasonic welding for thermoplastics. *J Thermoplast Compos Mater* 23:647–664